Bioconjugate Chemistry

Article

pubs.acs.org/bc

Interrogating the Role of Receptor-Mediated Mechanisms: Biological Fate of Peptide-Functionalized Radiolabeled Gold Nanoparticles in Tumor Mice

Francisco Silva,[†,○] Ajit Zambre,[∥,○] Maria Paula Cabral Campello,[*,†] Lurdes Gano,[†] Isabel Santos,[†] Ana Maria Ferraria,[‡] Maria João Ferreira,[§] Amolak Singh,[∥] Anandhi Upendran,[⊥] António Paulo,[*,†] and Raghuraman Kannan[*,∥,#,▽]

[†]Centro de Ciências e Tecnologias Nucleares, Instituto Superior Técnico, Universidade de Lisboa, Lisbon, Portugal

[‡]Centro de Química-Física Molecular, Instituto Superior Técnico, Universidade de Lisboa, Lisbon, Portugal

[§]Centro de Química Estrutural, Instituto Superior Técnico, Universidade de Lisboa, Lisbon, Portugal

[∥]Departments of Radiology, [⊥]MU-iCATS, [#]BioEngineering, and [▽]International Center for Nano/Micro Systems and Nanotechnology, University of Missouri, Columbia, Missouri 65211, United States

Supporting Information

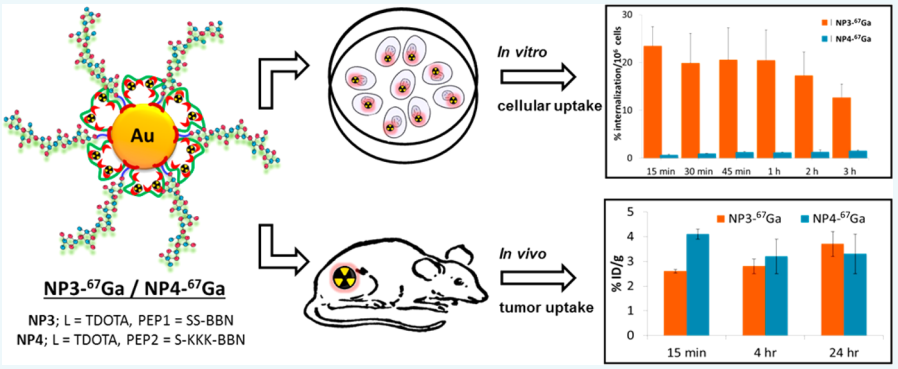

ABSTRACT: To get a better insight on the transport mechanism of peptide-conjugated nanoparticles to tumors, we performed *in vivo* biological studies of bombesin (BBN) peptide functionalized gold nanoparticles (AuNPs) in human prostate tumor bearing mice. Initially, we sought to compare AuNPs with thiol derivatives of acyclic and macrocyclic chelators of DTPA and DOTA types. The DTPA derivatives were unable to provide a stable coordination of ^{67}Ga, and therefore, the functionalization with the BBN analogues was pursued for the DOTA-containing AuNPs. The DOTA-coated AuNPs were functionalized with BBN[7−14] using a unidentate cysteine group or a bidentate thioctic group to attach the peptide. AuNPs functionalized with thioctic-BBN displayed the highest *in vitro* cellular internalization (≈ 25%, 15 min) in gastrin releasing peptide (GRP) receptor expressing cancer cells. However, these results fail to translate to *in vivo* tumor uptake. Biodistribution studies following intravenous (IV) and intraperitoneal (IP) administration of nanoconjugates in tumor bearing mice indicated that the presence of BBN influences to some degree the biological profile of the nanoconstructs. For IV administration, the receptor-mediated pathway appears to be outweighed by the EPR effect. By contrast, in IP administration, it is reasoned that the GRPr-mediated mechanism plays a role in pancreas uptake.

INTRODUCTION

Targeting nanoparticles selectively to the tumor site remains a significant challenge. To overcome this challenge, several research studies focused on understanding the transport mechanism of nanoparticles to the tumor.[1−8] Two types of mechanisms, passive and active targeting, are reported in the literature to explain the delivery of nanoparticles to the tumor.[9] Passive targeting is based on the leakiness characteristics of the tumor; whereas, active targeting is based on the receptors that are overexpressed on the tumor. Nanoparticles choose either one or both of these mechanisms to reach the tumor site. Previous studies demonstrate that numerous parameters influence the choice of mechanism for *in vivo* delivery of nanoparticles to tumors.[4,10−15] Several endogenous parameters including size, charge, and surface-bound ligand play significant roles in deciding the mechanism of delivery of nanoparticles.[4,10−15] In addition, exogenous factors such as reticuloendothelial system (RES) sequestration and biocorona

Received: February 22, 2016
Revised: March 18, 2016
Published: March 22, 2016

DOI: 10.1021/acs.bioconjchem.6b00102
Bioconjugate Chem. 2016, 27, 1153−1164

Scheme 1. Synthesis of TDOTA[a]

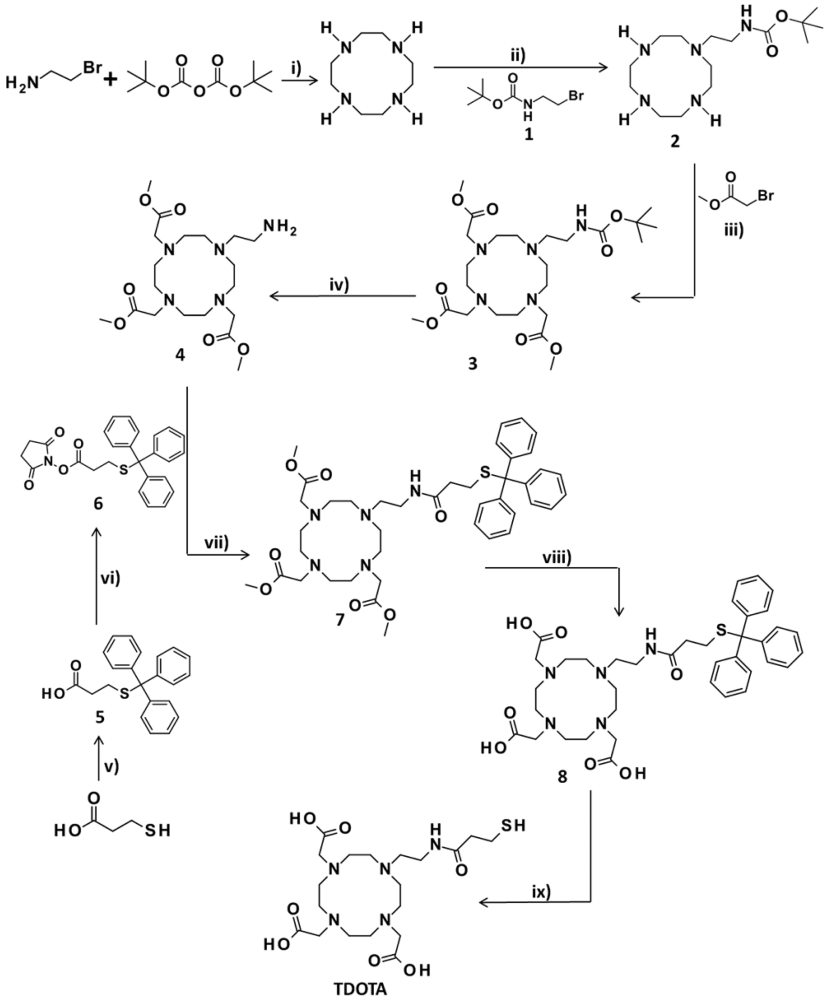

[a]Reactions and conditions: (i) MeOH, 24 h, RT; (ii) toluene, 24 h, reflux; (iii) CH_3CN, Na_2CO_3, 8 h, 70 °C; (iv) TFA/CH_2Cl_2, 2 h, RT; (v) THF, Ph_3CSH, NaH, 30 min, RT; (vi) CH_2Cl_2, NHS, EDC, DIPEA, 24 h, RT; (vii) DMF/CH_2Cl_2, DIPEA, 24 h, RT; (viii) THF/MeOH/H_2O, LiOH, 24 h, RT; (ix) TFA/H_2O/thioanisole/1,2-dithiolethane, 2 h, RT.

formation are also responsible in the transport mechanism of NPs to tumor.[16,17] With regard to passive targeting, Xia and co-workers have demonstrated that 30 nm gold cages performed better *in vivo* when compared with 55 nm nanocages.[18] In sharp contrast, Chan and co-workers have shown that smaller sized gold nanoparticles (20 nm) exhibit a lower degree of tumor accumulation than did 100 nm particles.[19,20] These studies further demonstrate that multiple factors in addition to size play a role in deciding the final *in vivo* destination of nanoparticles in passive targeting. A similar observation is noted in the case of active targeting. Several novel approaches were developed for directing the nanoparticles toward receptors that are overexpressed on the surface of the tumor. A variety of biomolecules including antibodies, ScFv fragments, affibodies, peptides, aptamers, and carbohydrates have been attached to nanoparticles and their selective uptake in tumors studied.[4−6,8,21−25] Even though these approaches are relatively successful, it is not yet clear that surface bound biomolecules have a convincing role in targeting the tumor. Pioneering work by Park and co-workers demonstrate that antibody targeted liposomes have not shown any increase in tumor uptake when compared with the nontargeted liposomes.[26] Nevertheless, Davis and co-workers have demonstrated that targeted nanoparticles showed enhanced efficacy than the nontargeted analogue.[27] As noted above, the ground rules for developing a successful targeted nanoparticles are still emerging.

To obtain further insight on the role of surface bound biomolecules in targeted delivery, herein we have systematically studied the *in vivo* tumor targeting characteristics of radiolabeled gold nanoparticles (AuNPs) covalently conjugated with bombesin peptides. Bombesin (BBN) peptide recognizes gastrin releasing peptide (GRP) receptors that are overexpressed in a variety of human tumors including prostate, breast, and lung cancer.[28−31] In this study, the *in vivo* tumor uptake of these AuNPs is studied in prostate tumor bearing mouse models using Ga-67 as the radiolabel. ^{67}Ga is a γ-emitting radionuclide that presents physical properties suitable for *in vivo* imaging by single photon emission computed tomography (SPECT); moreover, the congener ^{68}Ga is an emerging positron emitter with increasing clinical relevance, namely, for tumor imaging by positron emission tomography (PET).[32] For radiolabeling, gallium-chelating ligands DTPA or DOTA were surface attached aiming at a fast and stable coordination of ^{67}Ga. Before proceeding with the functionalization of the nanoparticle surface with the targeting peptides, it has been investigated if each type of ligand was able to achieve the

DOI: 10.1021/acs.bioconjchem.6b00102
Bioconjugate Chem. 2016, 27, 1153−1164

Scheme 2. Synthesis of the Nontargeted Nanoconstructs Stabilized with DTDTPA or TDOTA and the Respective Peptide Conjugated and/or Radiolabeled Particles

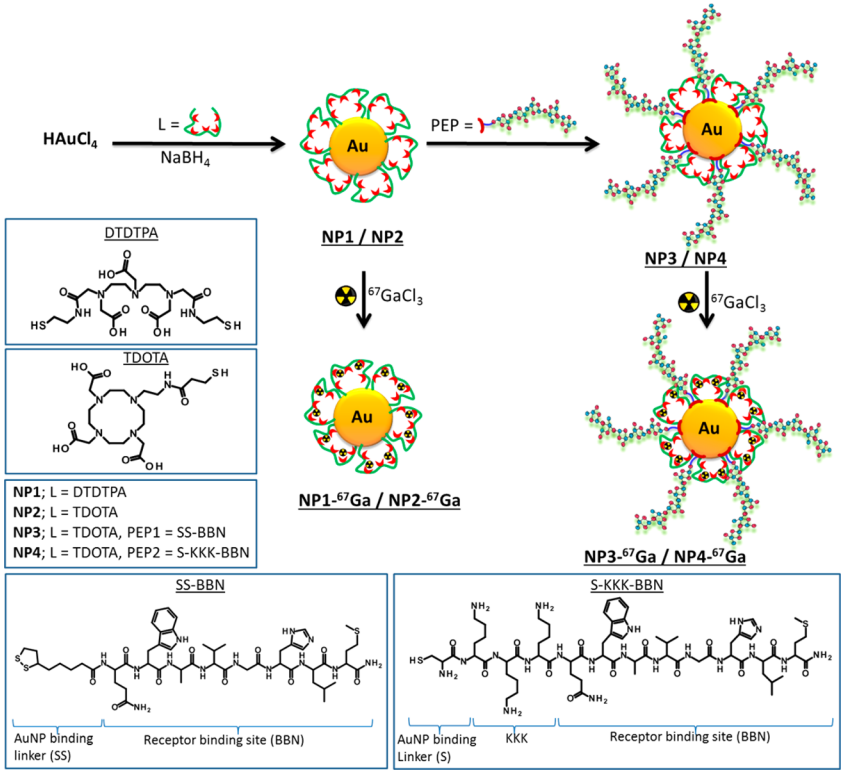

desired stable coordination of ^{67}Ga. To confirm that active targeting plays a crucial role, receptor-blocking studies were performed. We studied whether the route of administration, intravenous and intraperitoneal, plays any role in active targeting mechanism. Our previous studies were focused more on *in vitro* demonstration of nanoconjugates in recognizing receptors on the cell surface, and peptide conjugated gold nanoparticles internalize primarily via receptor-mediated endocytosis.[2,33] In addition, we have also shown that radioactive bombesin gold nanoconjugates (^{198}AuNPs) localize in the pancreas and have poor uptake in tumors in mice models.[1] In the present study, we report the following results: (i) design, synthesis, and characterization of ^{67}Ga-labeled targeted AuNPs; (ii) understanding the *in vitro* stability, GRP receptor recognition, and internalization efficacy of targeted AuNPs in human cancer cells; (iii) measuring the quantitative biodistribution of nanoparticles in tumor bearing mice models; (iv) comparing uptake of targeted nanoparticles in tumor mice by blocking receptors; and (v) evaluating the route of administration of nanoparticles for optimal tumor uptake.

RESULTS AND DISCUSSION

It is important to design a robust and tunable nanoconstruct to effectively study the mechanism of tumor uptake in mice models. We have set out to obtain a library of BBN targeted ^{67}Ga-labeled nanoparticles of the general formula [AuNP(L)-(R)], where L represents a polyamino carboxylic chelator, and R can be a BBN derivative. These nanoconstructs would contain three important components. (i) Component 1 (AuNPs): the nanoparticle core comprised rigid small core (3−5 nm) sized gold nanoparticles (AuNPs). The variation in core size was minimized throughout the study. Several investigations have demonstrated that AuNPs are nontoxic, nonimmunogenic, and are ideally suited for our study. (ii) Component 2 (L): We investigated both DTPA and DOTA as ligands (L) for irreversibly chelating ^{67}Ga and the surface anchored to AuNPs. L contains both the "SH" group and amino carboxylates for attaching with AuNP and to chelate ^{67}Ga, respectively. The radiolabeling method was chosen for performing quantitative *in vivo* biodistribution studies since the measurement of radioactivity is a much more reliable method than the elemental analysis of gold (e.g., by fAAS, ICP, or NAA). However, it is important to ensure irreversible attachment of the radionuclide to the surface of the nanoparticle. (iii) Component 3 (BBN): the targeting molecule chosen for the study is a receptor-avid peptide, a bombesin derivative. Our rationale for choosing BBN is as follows: GRP receptors (called bombesin type 2 (BB_2) receptor) have high affinity for its natural ligand, bombesin (BBN). Several clinical studies have shown that BBN analogues have superior targeting characteristics.[34−36]

The ligand framework, DTPA or DOTA, was attached on the surface of the nanoparticle by a stable thiol bond. Such proximity between the ligand and nanoparticle provides rigidity and enhanced stability to the final construct. Several research studies have shown that both DTPA and DOTA are excellent chelating ligands for stabilizing Ga-67 in both molecular or nanosized frameworks.[37−40] As such, both DTPA and DOTA ligands lack chemical functionality to directly attach with gold atoms. Hence, we devised synthetic strategies to incorporate thiol groups in the ligand structure being aware that the modification of these polyamine chelators (L) can influence the *in vivo* stability of ^{67}Ga-L that directly depends on the coordination saturation and *trans*-chelation with transferrin.

DOI: 10.1021/acs.bioconjchem.6b00102
Bioconjugate Chem. 2016, 27, 1153−1164

Table 1. Physico-Chemical Characterization of Nanoconjugates Synthesized in the Present Study

nanoparticle[a]	UV−vis (nm)	TEM (nm)	hydrodynamic size (nm) (PDI)	zeta-potential (mV)
NP1	520	2.28 ± 1.32	100.6 (0.111)	−80.7 ± 15.6
NP2	520	4.29 ± 1.60	20.6 (0.342)	−62.6 ± 18.6
NP3	520	4.79 ± 1.50	22.5 (0.420)	−60.5 ± 16.4
NP4	520	4.04 ± 1.52	47.35 (0.370)	−30.1 ± 16.8

[a]All measurements were performed by preparing the nanoparticle solution in DI water (≈pH 6).

We have focused on the already described thiolated DTPA derivative 2-[bis[2-[carboxymethyl-[2-oxo-2-(2-sulfanylethylamino)ethyl]amino]ethyl]amino]acetic acid (**DTDTPA**) and on a new thiolated DOTA derivative. This new DOTA derivative, trimethyl 2,2′,2″-(10-2(3-(tritylthio)-propamido)ethyl)-1,4,7,10-tetraazacyclododecane-1,4,7-trityl)-triacetate (**TDOTA**), relied on the introduction of a single 2-ethylamine group in the cyclen framework, for further coupling to a thiolated pendant arm (Scheme 1). The synthesis of **TDOTA** started with the N-alkylation of cyclen by reaction with *tert*-butyl *N*-(2-bromoethyl) carbamate (**1**). The resulting monoalkylated cyclen derivative (**2**), containing a BOC protected pendant arm, was treated with methyl 2-bromoacetate to afford **3**. Then, removal of the BOC protecting group from **3** with TFA gave compound **4** displaying a terminal amino function for coupling of 3-mercaptopropionic acid. Treatment of **4** with a NHS activated ester of 3-mercaptopropionic acid (**6**), having the terminal thiol protected with a trityl group, yielded the amide derivative **7**. Basic hydrolysis of the methyl ester functions of **7** followed by acid deprotection of the trityl protecting groups led to the desired final compound.

Synthesis of Targeted and Nontargeted Nanoconstructs. For synthesizing the nanoconstructs, we developed a stepwise ligand/peptide incorporation methodology. In the first step, the ligand framework was attached to the surface of AuNPs using the thiol groups of the modified DOTA or DTDTPA. A previously developed procedure was used to attach the DTPA derivative (**DTDTPA**) onto the surface of AuNPs, which led to the **AuNP-DTDTPA** (**NP1**) nanoconstructs (Scheme 2).[41−44] Details of the synthetic procedure are presented in the Experimental Procedures (see Supporting Information). Similar to **NP1**, the strategy for the synthesis of the AuNPs stabilized with **TDOTA** was also based on the modified procedure of Brust et al.[45] As shown in Scheme 2, this involved the reduction of $HAuCl_4{\cdot}3H_2O$ with $NaBH_4$ in the presence of **TDOTA** using a molar ratio of 1:2.5 (Au/TDOTA) that resulted in the formation of a dark brown solution of DOTA stabilized gold nanoconstructs designated as **AuNP-TDOTA** (**NP2**). AuNP-L (L = **DTDTPA** and **TDOTA**) were purified by centrifugation methods, washed, and used for the subsequent steps.

As a next step, we focused on synthesizing radiogallium conjugates of **NP1** and **NP2** by reacting the nanoconstructs with $^{67}GaCl_3$. We optimized the procedure by radiolabeling nanoconjugates at different pH and reaction times. In a typical reaction, **NP1** or **NP2** (0.1 mg) was dissolved in acetate buffer at pH 7 and mixed with $^{67}GaCl_3$ (70−120 MBq) in 0.1 M HCl, and the reaction mixture was left undisturbed at 50 °C. Each reaction mixture was purified by ultrafiltration and the respective radiolabeled conjugate analyzed using radio-TLC. The radio-TLC control provided quantifiable data on the radiochemical yield and purity. The final ^{67}Ga-labeled nanoconstructs **NP1-^{67}Ga** and **NP2-^{67}Ga** were obtained with radiochemical yields of 86 and 88%, respectively, and with a radiochemical purity >95%.

It is important to study the stability of the radiolabeled **NP-^{67}Ga** conjugates in the presence of biologically relevant media and apo-transferrin. Ga-67 attached to a weakly stable chelate is susceptible to trans-chelation with apo-transferrin, resulting in the leaching of gallium from the chelate. Thus, this test acts as an independent measure to evaluate the stability of the nanoconjugate. For the stability studies, **NP-^{67}Ga** nanoconjugates were suspended in 0.1 M PBS, NaCl 0.9%, cell culture medium, and apo-transferrin (3 mg/mL, in 10 mM $NaHCO_3$) and incubated at 37 °C. At different intervals of time, a small amount of solution was removed and analyzed using radio-TLC (up to 24 h). The details are presented in a graph (ESI-Figure 6). The ^{67}Ga-labeled nanoconstruct functionalized with **DTDTPA** (**NP1-^{67}Ga**) showed poor stability in apo-transferrin when compared to the one functionalized with **TDOTA** (**NP2-^{67}Ga**). In addition, **NP2-^{67}Ga** has shown a moderate to high stability in all biological media, although there is some decrease in the percentage of radiolabeled nanoconstruct for the shortest incubation times. For longer incubation times, however, such a percentage remained fairly constant. Because of the inability of **NP1** to provide a stable coordination of Ga-67, we did not use this nanoplatform for further functionalization with the BBN peptides. The observed instability would lead to unreliable data regarding the biological profile of the corresponding BBN-conjugated AuNPs when performing cellular (*in vitro*) and animal (*in vivo*) studies, due to a high probability that the radioactivity distribution would not reflect that of the nanoparticles.

After confirming that the AuNP-TDOTA (**NP2**) nanoconstruct possesses suitable coordinating properties to attach Ga-67, **NP2** was functionalized with BBN peptides. We used two different BBN analogues in our study (SS-BBN and S-KKK-BBN; Scheme 2). In both the analogues the amino acid sequence BBN[7−14] remains unaltered; however, the functional group that allows for the binding to the gold surface is altered. In SS-BBN, the thioctic acid group ligates with nanoparticles, while for S-KKK-BBN, it was through cysteine-SH. We hypothesized that cysteine would allow increased loading of peptide on AuNPs. The possibility of increasing the peptide loading was expected to enhance the targeting ability of the BBN-containing AuNPs.

We used a 1:2 ratio (w/w) of AuNP/BBN for functionalizing **NP2** (Scheme 2), both with SS-BBN and S-KKK-BBN, to obtain **NP3** and **NP4**, respectively. After the reaction, the amount of unreacted BBN analogues was estimated using HPLC. The concentration of SS-BBN attached in **NP3** was 0.86 μmol (0.98 mg), while the amount of S-KKK-BBN attached in **NP4** was 0.17 μmol (0.24 mg) per mg of nanoparticle. As mentioned above, the conjugation of S-KKK-BBN to the AuNPs involves uniquely the formation of one Au−S bond, and therefore, the coupling of the same number of

DOI: 10.1021/acs.bioconjchem.6b00102
Bioconjugate Chem. 2016, 27, 1153−1164

peptide molecules involves less number of gold atoms if compared with SS-BBN. This is why one could expect that it should be possible to attach a high number of peptide molecules to the AuNPs in the case of S-KKK-BBN. However, the involvement of two sulfur atoms per molecule in the conjugation of SS-BBN to the AuNPs can lead to a more stable binding, which eventually justifies the higher payload that has been achieved in the case of this BBN derivative. The characterization details of these BBN-containing nanoconjugates and respective precursor AuNPs (UV−visible, TEM analysis, charge and hydrodynamic size distribution, XPS, proton, and HSQC NMR) are presented in Supporting Information (ESI-Figure 1−ESI-Figure 5; Table 1; and ESI-Table 1).

Nanoconstructs **NP3** and **NP4** were successfully radiolabeled with Ga-67 following the same procedure described previously for **NP2** (Table 2). The resulting nanoparticles, **NP3-^{67}Ga** and **NP4-^{67}Ga**, were obtained with radiochemical yields of 69% and 71%, respectively, and with a radiochemical purity >95%.

Table 2. Reaction Conditions for the ^{67}Ga-Labeling of Nanoconjugates and Respective Radiochemical Yields

nanoparticle	temperature (°C)	reaction time (min)	radiochemical yield (%)
NP1-^{67}Ga	50	15	86
NP2-^{67}Ga	50	30	89
NP3-^{67}Ga	50	30	69
NP4-^{67}Ga	50	30	71

The stability of **NP3-^{67}Ga** and **NP4-^{67}Ga** was studied in the presence of relevant biological media and apo-transferrin (ESI-Figure 6). Overall, **NP3** and **NP4** maintain a moderate to high stability as seen previously for their precursor **NP2**. However, among these radiolabeled DOTA conjugated **NP2-NP4**, **NP4** showed the least stability. Nevertheless, more than 60% of **NP4-^{67}Ga** did not release ^{67}Ga even after 24 h of incubation with the cell medium. It is possible that the positively charged amino acids (lysine) present in the peptide backbone of **NP4** repel with positively charged gallium ions in close proximity resulting in their leaching. Gallium ions farther from lysine residues are stably coordinated and stay intact with no release during the study period.

Receptor Affinity and Cellular Uptake of NP3 and NP4. We used a competitive binding assay to estimate the specificity of BBN conjugated nanoconstructs to GRP receptors overexpressed on the surface of cancer cells. In this assay, the ability of the nanoparticles to displace the radioiodinated specific binding ligand was estimated. We used ^{125}I-Tyr$_4$-BBN as the radioligand to assess the affinity of **NP(2−4)** in human prostate cancer cells (PC3). (Figure 1). As expected, **NP3** and **NP4** display a significant affinity toward GRP with IC_{50} values of 0.045 ± 0.003 and 0.160 ± 0.027 μg/mL, respectively. In a similar fashion, **NP2** showed no affinity for GRP receptors. Among all of the nanoconjugates, **NP3** has a lower IC_{50}, and it can be attributed to the increased number of BBN peptides present in this construct.

One of the crucial experiments to measure the specificity of radiolabeled nanoconjugates toward GRP receptors involves understanding the internalization pattern. We performed receptor uptake studies in GRPr-positive human prostate cancer PC3 cells by exposing the cells to a solution of the radiolabeled NPs (**NP(2−4)-^{67}Ga**) in cell culture medium and

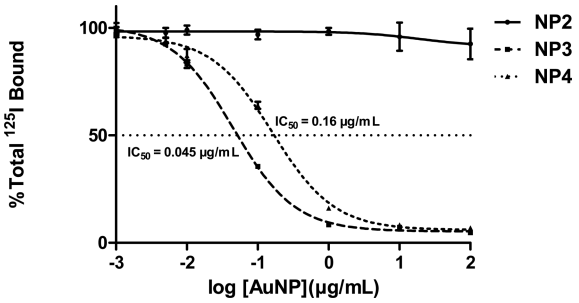

Figure 1. Representative binding affinity (mean ± SD, n = 4) of nanoconjugates **NP2**, **NP3**, and **NP4** in PC-3 cells by competitive assays with ^{125}I-Tyr$_4$-BBN.

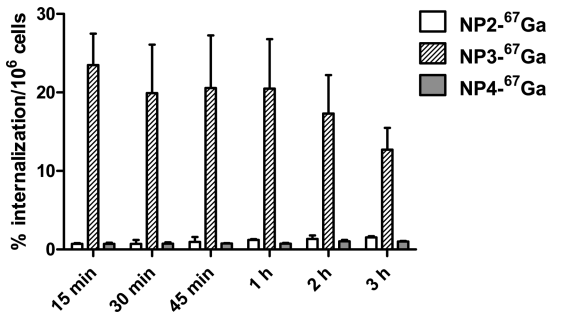

Figure 2. Cellular uptake (mean ± SD, n = 4) of **NP2-^{67}Ga**, **NP3-^{67}Ga**, and **NP4-^{67}Ga** in PC3 cells, after incubation at 37 °C at different intervals of time. Internalization is expressed as the percentage of the applied radioactivity internalized by the cells.

incubating at 37 °C for different intervals of time (Figure 2). The internalization observed for **NP2** and **NP4** showed a similar profile with a slow uptake reflected from the increase in radioactivity that reaches relatively low plateau values (<2%). By contrast, **NP3-^{67}Ga** has shown a very high and rapid internalization into the cells with almost 25% internalization after 15 min of incubation; thereafter, there is a slow decrease in the uptake of radioactivity suggesting the release of the Ga ions from the cells. As stated before, the peptide load of **NP3** is roughly 5-fold higher than that of **NP4**, which is certainly related to the trend observed for the cellular internalization as well as for the binding affinities of the nanoconstructs toward GRPr in PC3 cells. Altogether, these findings indicated that the internalization of **NP3-^{67}Ga** should involve a receptor-mediated process. To further confirm that **NP3-^{67}Ga** is retained within PC3 cells, we investigated the efflux of radioactivity from the cell. Typically, **NP3-^{67}Ga** was incubated in PC3 cells for 15 min, and the unbound nanoconjugates were washed. The radioactivity retained by the cells was measured. Then, the medium was replaced with culture medium without any radioactive compound, and the radioactivity release was monitored at different intervals of time by washing and measuring the radioactivity associated with the cells again. A fast washout of the radioactivity has been observed during the first 2 h. However, thereafter, the efflux rate significantly decreases, and the activity present in the cells remains essentially constant after 4 h of incubation, reaching roughly 40% of the initial radioactivity (ESI-Figure 8). Therefore, one can consider that the PC3 cells retained a reasonable amount of **NP3-^{67}Ga**, which was an encouraging result to further study the targeting ability of these AuNPs in GRP receptor positive tumors.

DOI: 10.1021/acs.bioconjchem.6b00102
Bioconjugate Chem. 2016, 27, 1153−1164

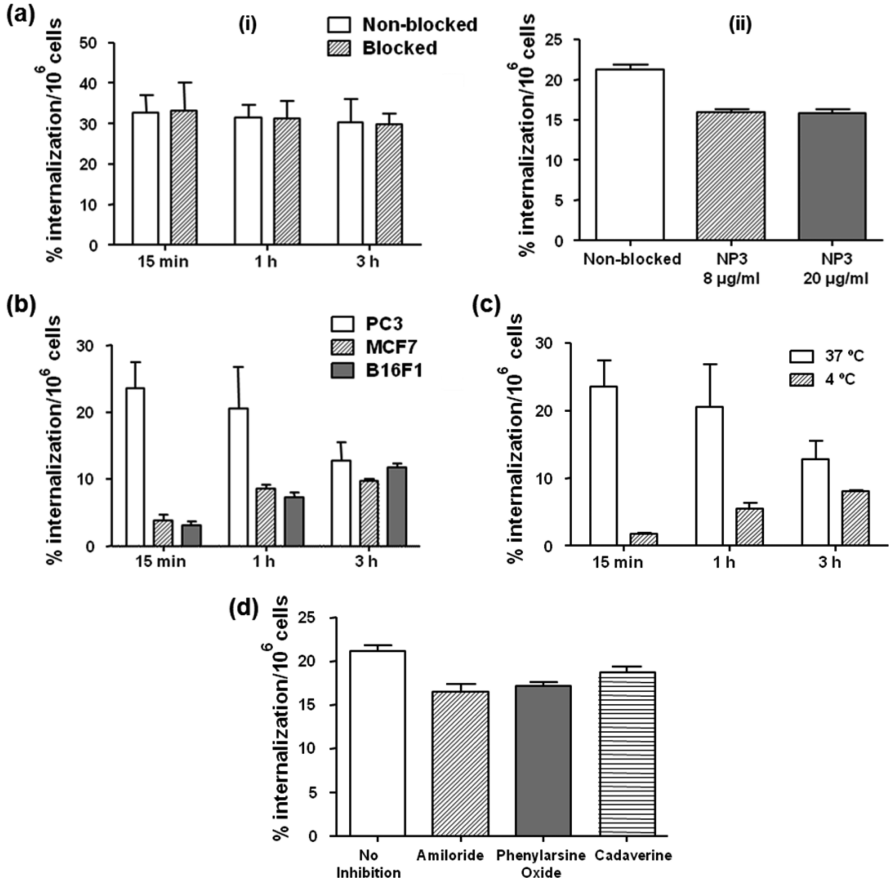

Figure 3. (a) Cellular uptake (mean ± SD, n = 4) of **NP3-^{67}Ga** at 37 °C in PC3 cells in the presence and absence of (i) BBN (1 μM/well) and (ii) cold **NP3** (8 μg/mL and 20 μg/mL per well). (b) Comparative cellular uptake (mean ± SD, n = 4) for **NP3-^{67}Ga** at 37 °C in PC3, MCF7, and B16F1 cell lines. (c) Comparison of cellular uptake of **NP3-^{67}Ga** at 37 and 4 °C in PC3 cells. (d) Cellular uptake of **NP3-^{67}Ga** in the presence of amiloride, phenylarsine, and cadaverine at 37 °C in PC3 cells. Internalization is expressed as the percentage of the applied radioactivity internalized by the cells.

Mechanism of Cellular Internalization of the NP4-^{67}Ga Conjugate. As the focus of this study is to understand whether peptide conjugated nanoparticles undergo an active targeting mechanism, we have performed a very systematic study to evaluate the mechanism of uptake of **NP3-^{67}Ga** in GRPr expressing PC3 cells. Several studies described above demonstrate that **NP3-^{67}Ga** exhibits high stability, cellular internalization, and retention. Therefore, our mechanistic studies were performed utilizing only this conjugate. We performed four experiments using **NP3-^{67}Ga**: (i) evaluate the effect of internalization of **NP3-^{67}Ga** after blocking the receptors with free peptide or cold **NP3**; (ii) compare the internalization of **NP3-^{67}Ga** in GRP receptor positive (PC3) and GRP receptor negative cells lines (human breast cancer MCF7 and mouse melanoma B16F1 cell lines); (iii) evaluate the energy dependence of the **NP3-^{67}Ga** in internalization; and (iv) evaluate the effect of internalization of **NP3-^{67}Ga** in the presence of cellular pathway blockers. First, GRP receptors on PC3 cells were blocked using free BBN and subsequently incubated with **NP3-^{67}Ga**. Thereafter, the amount of nanoparticles internalized at different time intervals was quantified (Figure 3a (i)). These studies showed that there is no significant difference in the amount of internalized radioactivity between the blocked and the nonblocked cells. The presence of BBN on the surface of the AuNPs clearly influences its internalization into the cells, but apparently, the process involved is not mediated merely by the specific interaction with GRPr, as indicated by the inability of cold free BBN peptide to inhibit the uptake. It was hypothesized that the moderately large hydrodynamic size of **NP3** (22.5 nm (PDI = 0.420)) could contribute for an easier saturation of the GRPr receptors in the cell membrane. As invoked by other authors, due to their size, a single nanoparticle can block the access to several receptor molecules, even without being involved in direct and specific interactions with such molecules.[46] On the flip side, a single **NP3** having several copies of the bioactive peptide can specifically interact with more than one GRP receptor, leading to a strong binding as found often for multimerized constructs, due to the so-called concept of avidity.[47] For all these reasons, monomeric BBN can be a less effective competitor in the GRP binding of **NP3-^{67}Ga** if compared with the cold **NP3** itself. Therefore, blockade experiments using increasing concentrations of cold **NP3** were performed (Figure 3a (ii)). No significant decrease of the amount of internalized radioactivity was observed, even using a 5-fold greater concentration of **NP3**, compared to the concentration of the radiolabeled AuNPs. It should also be taken into account that due to the low amount of ^{67}Ga present in the radiolabeling mixture ($<4.7 \times 10^{-9}$ mmol), it is common to have nonradiolabeled AuNPs in the final **NP3-^{67}Ga** solution. These nonradiolabeled AuNPs will compete for the binding with GRP receptor. So far, the separation of the radiolabeled AuNPs from the nonradiolabeled ones was not possible with the available methodologies. In summary, blocking the GRP

DOI: 10.1021/acs.bioconjchem.6b00102
Bioconjugate Chem. 2016, 27, 1153−1164

receptors on the surface does not affect internalization of **NP3-^{67}Ga** in PC3 cells. Second, internalization ability of **NP3-^{67}Ga** was investigated in both GRP receptor positive (PC3) and negative cell lines (human breast cancer MCF7 and mouse melanoma B16F1). It is observed that the initial rate of internalization is significant for the GRP positive PC3 cells (with >20% of internalization observed), whereas in the GRP receptor negative cell lines less than 5% of internalization was observed at 15 min of incubation. Moreover, there is a slow decrease in radioactivity from PC3 cells upon increasing incubation time, while a reverse trend, i.e., a steady increase of internalization with the time of incubation was observed for the MCF7 and B16F1 cell lines. These results are indicative that the presence of GRPr influences the cellular uptake of the nanoparticles, taking into account the much faster internalization observed for the PC3 cells (Figure 3b). Altogether, these results prompt us to presume that the cellular internalization of **NP3-^{67}Ga** in PC3 cells is fairly mediated by the GRP receptors. Third, in order to gain more insight into the involvement of different energy dependent pathways in the internalization of **NP3-^{67}Ga** in PC3 cells, cellular uptake was monitored at two different temperature conditions. The uptake of **NP3-^{67}Ga** in PC3 cells at 4 °C is less than that at 37 °C; these results confirm that its cellular uptake involves energy dependent mechanisms, like phagocytic and endocytic pathways (Figure 3c). Similar results are observed in our previous study on BBN conjugated gold nanocages; these cages showed decreased cellular uptake at 4 °C in GRP expressing cancer cells.[33]

Fourth, to investigate if the cellular internalization pathway is dependent on receptor-mediated endocytosis, cellular uptake was monitored in the presence of inhibitors of different cellular transport processes such as amiloride, phenylarsine oxide, or cadaverine (endocytosis or phagocytosis inhibitors). These inhibitors decreased the cellular uptake of **NP3-^{67}Ga** up to 20% in PC3 cells (Figure 3d). Amiloride is a Na^+/H^+ channel inhibitor that is known to block macropinocytosis and phagocytosis pathways that correspond to nonreceptor-mediated pathways. Phenylarsine oxide or cadaverine, are both clathrin-mediated endocytosis (CME) inhibitors. In general, receptor based internalization of molecules involves clathrin machinery.[48] These results indicate that the uptake of **NP3-^{67}Ga** occurs most probably via active phagocytic and endocytic pathways, which in the latter case might involve the internalization of GRPr. Recently, we have shown that the uptake in PC3 cells of BBN-containing gold nanocages is mediated by CME and confirmed the formation of characteristic clathrin coated pits with lysosomal release of the nanocages.[33] For **NP3-^{67}Ga**, the cellular uptake mechanistic study was not so detailed, and other internalization possibilities including other endocytic transport processes, namely, caveolae (lipid transport) or alternative pathways, need to be investigated. As proposed by other authors, the involvement of these alternative pathways may result from the aggregation of the individual nanoparticles since clathrin mediation is size dependent.[33,49,50] In fact, it is considered that nanoparticles can utilize CME to internalize the cells when their dynamical aggregates are not superior to a 300 nm size limit.[33] As the hydrodynamic size of **NP3** was 22.5 nm (PDI = 0.420), it is conceivable that the internalization of **NP3-^{67}Ga** will occur through CME, with involvement of GRP, only when these AuNPs present themselves to the cell surface as individual "monomeric" nanoparticles.

***In Vivo* Studies.** It is important to understand the biodistribution of nanoconjugates in tumor bearing mice before initiating mechanistic studies. Previous studies demonstrate that the nanoparticles preferentially accumulate in RES organs, the liver and spleen. For example, Ga-67 labeled dextran-coated iron oxide showed 75% of ID accumulated in the liver and spleen after 15 min post-injection.[40] Our previous investigation showed that gum arabic coated radioactive gold nanoparticle accumulates in liver and spleen.[51] Of interest to the present study, we have demonstrated that gold nanoparticle−bombesin conjugates accumulate more than 50% ID/g in the liver and spleen.[1] If the size of the nanoparticles is large, accumulation in lungs also predominates; however, smaller sized particles excrete via urine.[52] As noted in previous sections, size alone does not dictate the fate and distribution of nanoparticles *in vivo*. Other factors such as charge, surface coating, zeta potential, and protein corona around nanoparticles play crucial roles in their accumulation and excretion. In addition to the above, radiolabeled conjugates should establish *in vivo* structural integrity for effective uptake. Poor stability leads to the release of the radiolabel from the conjugate resulting in diminished uptake in target organs and thus would lead to wrong conclusions being drawn. Liu and co-workers have shown that Cu-64 alloyed gold nanoparticles showed uptake in the spleen, instead of the liver, due to a release of the radiolabel and formation of smaller size particles.[53] Smaller sized radiolabeled particles were filtered by the spleen, and they used biodistribution data as a tool to establish the *in vivo* stability. In the present study, the structural integrity of the nanoconjugate was evaluated by measuring the uptake of radioactivity in RES and other nontarget organs. Particularly, we investigated the biodistribution and tumor uptake of **NP3-^{67}Ga** and **NP4-^{67}Ga** (Figures 4 and 5; ESI-Table 2).

One of the important factors that represent the *in vivo* integrity of the nanoparticle is their uptake in RES organs. In general, most nanoconjugates show very high uptake in these organs, and therefore, it may serve as an independent parameter to evaluate their *in vivo* stability. For both ^{67}Ga labeled AuNPs reported herein (**NP3-^{67}Ga** and **NP4-^{67}Ga**), the general trend of the RES uptake remains similar for different time points, and the additional data are presented in the Supporting Information. At 4 h post-injection time point, **NP3-^{67}Ga** showed the lowest uptake in the liver and spleen (27.1 and 10.6% ID/g) when compared with that of **NP4-^{67}Ga** (61.9 and 12.7% ID/g). A recent study with Ga-68 labeled NOTA ligand conjugated to hydrophilic bombesin showed less than 5% ID/g uptake in the liver and spleen.[54] In another study, ^{67}Ga-DOTA-GABA-BBN showed less than 1% ID/g uptake in RES organs.[34] These studies confirm that small molecule BBN conjugates labeled with Ga-67 or Ga-68 show lower RES organ uptake, when compared with our ^{67}Ga labeled BBN-containing AuNPs.

To further evaluate the GRP receptor-targeting efficacy of the radiolabeled nanoconstructs, the uptake of NPs in the pancreas, tumor, and intestine were analyzed at different post-injection time points. It is known in the literature that the GRP receptor density in mice follow the order: pancreas > tumor > intestine, and consequently it is common to observe high uptake in the pancreas for BBN derivatives.[1,55] At 24 h post-injection (p.i.), the pancreas uptakes for **NP3-^{67}Ga** and **NP4-^{67}Ga** were 4.5 and 1.5% ID/g, respectively. Previous studies show that the Ga-68-NOTA-BBN conjugate has an uptake of ∼5% ID/g in the pancreas within 1 h of injection and that the ^{67}Ga-DOTA-GABA-BBN derivative showed 1.2% of

DOI: 10.1021/acs.bioconjchem.6b00102
Bioconjugate Chem. 2016, 27, 1153−1164

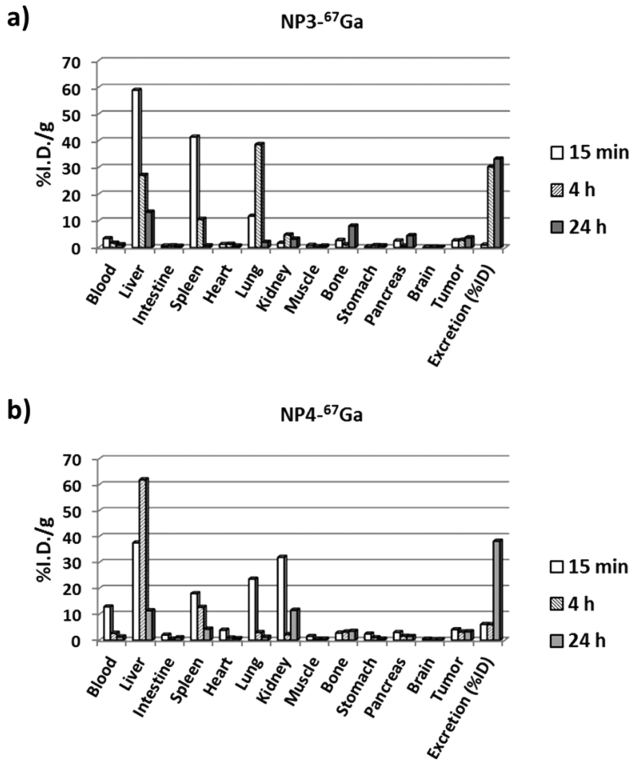

Figure 4. Biodistribution of (a) **NP3-^{67}Ga** and (b) **NP4-^{67}Ga** in tumor and organs in BALB/c nude mice bearing human prostate PC3 xenografts, injected intravenously via tail vein injection. Data are expressed as percentages of injected activity per gram of tissue (% ID/g), except for the GI tract, which is expressed as percentages of injected activity per organ. Error bars represent the mean ± standard deviation (n = 3).

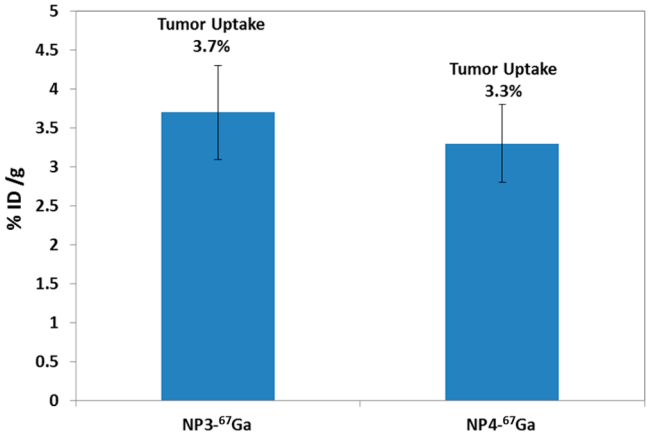

Figure 5. Comparison of tumor uptake of the BBN-containing radiolabeled nanoconstructs at the 24 h post-injection time point.

uptake.[34,54] A very high uptake of 27% ID/g was observed in the pancreas with ^{68}Ga-labeled NOTA-8-Aoc-BBN(7−14)NH_2.[56] In general, BBN conjugates showed 5 to 20% ID/g of uptake in GRP receptor overexpressing tissues.[1,57] When compared with these values, the uptakes observed for our nanoconjugates in the pancreas are relatively close to the low range values that have been found in the reported studies. Additional evidence for receptor targeting was obtained by comparing the tumor-uptake data of these conjugates. At 24 h p.i, **NP3-^{67}Ga** and **NP4-^{67}Ga** showed 3.7 and 3.3% ID/g of radioactivity uptake in tumors, respectively (Figure 5). ^{68}Ga-NOTA-BBN and ^{67}Ga-DOTA-GABA-BBN conjugates reported in the literature showed more than 8% and 1.2% ID/g in tumors, respectively.[34,54] Overall, nanoconstructs **NP3-^{67}Ga** and **NP4-^{67}Ga** display uptake in tumors in line with values found from other BBN compounds reported, although **NP3-^{67}Ga** showed a remarkably high cellular internalization compared to that of **NP4-^{67}Ga** that did not translate to the biodistribution profile. At this point, we had questioned whether it was EPR or receptor-mediated uptake mechanisms that was predominant for these nanoparticles. In order to answer this, further studies were performed and are described below.

Mechanism of Tumor Uptake. To unravel the mechanism of passive versus active tumor targeting by peptide-conjugated nanoparticles, we studied the uptake of nanoparticles in the pancreas and tumor in mice after blocking all non-EPR pathways. In our experiment, we blocked receptors in tumors by injecting free BBN in mice 30 min prior to the administration of nanoconjugates. After 4 h of administration, mice were sacrificed and the radioactivity measured in the pancreas and tumor (Figure 6). Our results indicate that blocking of GRP receptors by BBN showed no effect in the uptake of nanoconjugates in both of these organs. Between both nanoconstructs, **NP3-^{67}Ga** showed a decrease of ∼1% ID/g after blocking with BBN. The results suggest following important conclusions: (i) BBN peptide conjugated nanoparticles are not utilizing the receptor-mediated pathway as the primary route for targeting tumors; or (ii) the EPR pathway is dominant in the uptake of NPs in tumors. In addition to the above, the removal of nanoparticles by RES organs also plays a decisive role because the amount of nanoparticles accessible to tumors is largely limited.[3] The protein binding characteristics of nanoconjugates may also possibly decide the *in vivo* tumor uptake. Several reports have already suggested that the biomolecular corona around nanoparticles plays important roles in deciding the *in vivo* fate of the nanoparticle.[9,58] The protein corona becomes very relevant in nanoconjugates that are not functionalized with PEG on the surface, as PEG molecules prevent corona effects.[59] In fact, the preformed albumin corona has been utilized as a protective coating for the delivery of nanoparticles.[60] Dawson and co-workers have recently shown that the protein corona can significantly alter the targeting characteristics of nanoparticles.[61,62] In summary, even though targeting by bombesin nanoconjugates was achieved *in vitro*, the *in vivo* targeting efficacy was dampened possibly due to the exposure of nanoconstructs to the complex biochemical milieu.

BBN Nanoconjugates Recognize the GRP Receptor *in Vivo*. To evaluate whether the route of administration of nanoparticles in mice have any effect in minimizing protein corona formation which in turn would increase tumor uptake, we chose to administer the conjugate through i.p. route to mice. i.p. administrations of nanoconjugates provide immediate access due to the proximity of the injection site to GRP receptors present in pancreas. The i.p. administration route limits the exposure of nanoconjugates to the *in vivo* milieu and decreases the protein corona formation. Previous studies have shown that exposure time of nanoparticles to serum protein is also an important factor in protein corona formation.[61] Furthermore, i.p. administration would decrease the RES uptake and increase the accessibility of the concentration of nanoparticles to target organs. Therefore, we performed the following additional studies: (i) biodistribution of **NP3-^{67}Ga**

DOI: 10.1021/acs.bioconjchem.6b00102
Bioconjugate Chem. 2016, 27, 1153−1164

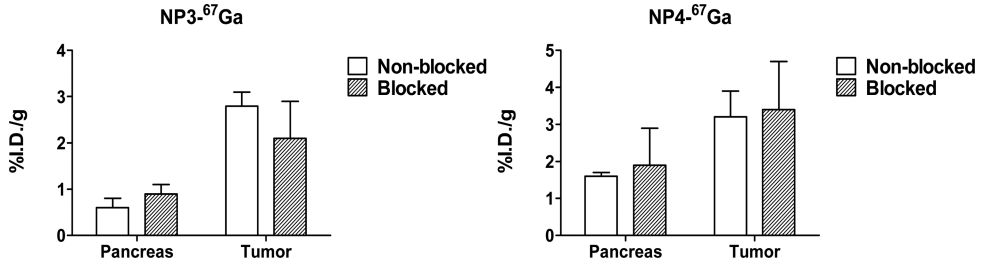

Figure 6. Uptake of NP3−67Ga and NP4−67Ga in the tumor and pancreas with and without blocking by bombesin in BALB/c nude mice bearing human prostate PC3 xenografts at 4 h post-injection. Error bars represent the mean ± standard deviation (n = 3). Statistical analysis of the data was done with GraphPad Prism, and the level of significance was set at 0.05. For the pancreas, p = 0.5434; for the tumor, p = 0.5677. Thus, the values are not significantly different.

after i.p. administration. We have selected **NP3-^{67}Ga** due to its augmented *in vitro* cell uptake, stability, and tumor uptake. (ii) Biodistribution of **NP2-^{67}Ga** after IP administration; and (iii) i.p. injection of **NP3-^{67}Ga** after blocking the receptors with bombesin (30 min prior to the injection of nanoconjugate).

The biodistribution profile of **NP3-^{67}Ga** after i.p. injection and IV administrations are different. In particular, the radioactivity uptake in the liver, spleen, and lung is significantly lower, with values <5% % ID/g for all of the post-injection times. Moreover, there is a significant pancreas uptake of 9.7 ± 1.6% ID/g at 4 h p.i.. The biodistribution profile of **NP2-^{67}Ga** can be considered similar but displayed a lower pancreatic uptake (5.6 ± 0.6% ID/g at 4 h p.i.). The tumor uptake for **NP3-^{67}Ga** after i.p. administration is only slightly higher when compared with tha of **NP2-^{67}Ga** (0.95 ± 0.03 vs 0.65 ± 0.11% ID/g at 24 h p.i.) (Figure 7; ESI-Table 3). Also, the tumor uptake is lower than that exhibited by the same nanoconjugates following IV administration (3.7 ± 0.5% ID/g at 24 h p.i.). Altogether, the study showed that there is a slight increase in the uptake of **NP3-^{67}Ga** in the pancreas. To understand whether this slight increase is receptor-mediated, we performed a receptor blocking experiment. In this experiment, the BBN peptide was injected IV, 30 min prior to the injection of **NP3-^{67}Ga** i.p.. As shown in Figure 8, there is a decrease (≈34%) of the pancreas uptake of **NP3-^{67}Ga**, when blocked with BBN. The result is in accordance with previously reported receptor saturating experiments utilizing antibody labeled nanoparticles. For example, Cai and co-workers have demonstrated that antibody conjugated radiolabeled silica nanoparticles showed an ∼30−40% decrease in tumor uptake upon saturating the receptors with free antibody.[63] These results suggest that uptake of **NP3-^{67}Ga** in the pancreas is possibly being mediated by GRP receptors but that other factors play a crucial role in tumor uptake. Nanoconjugates need to travel a longer distance to reach the tumor and would meanwhile encounter a large number of serum proteins. This is most likely the reason why i.p. administration leads to a lower tumor uptake in comparison to IV administration.

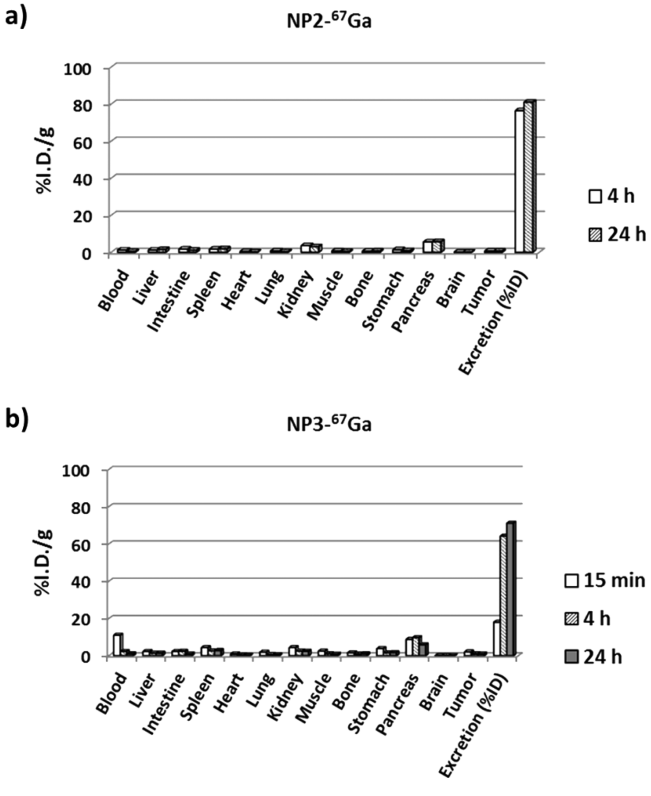

Figure 7. Biodistribution results (mean, n = 3; expressed as % ID/g of organ) for (a) **NP2-^{67}Ga** and (b) **NP3-^{67}Ga** after i.p. administration in BALB/c nude mice bearing human prostate PC3 xenografts.

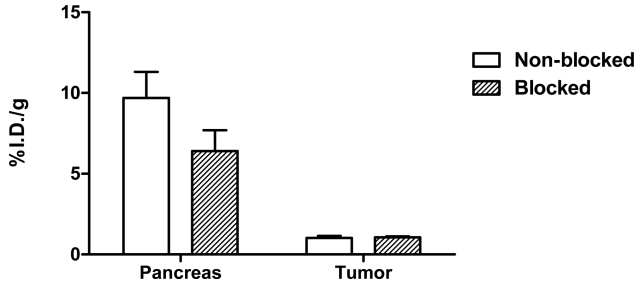

Figure 8. Comparison of the pancreas and tumor uptake (mean ± SD, n = 2; expressed as % ID/g of organ) for **NP3-^{67}Ga** after i.p. administration in BALB/c nude mice bearing human prostate PC3 xenografts, treated (blocked) or nontreated with BBN, at 4 h p.i.

CONCLUSIONS

Our initial work was focused on studying the ^{67}Ga-coordination capability of two distinct AuNPs platforms, one stabilized with a DTPA derivative (**NP1**) and another with a DOTA derivative (**NP2**). Nanoconstruct **NP1** lacks adequate capacity to maintain optimal Ga-67 coordination in the presence of biological media and apo-transferrin. However, **NP2** showed moderate to high stability, indicating that DOTA-containing AuNPs were optimal for Ga-67 delivery and hence were chosen for BBN-conjugation (**NP3** and **NP4**).

DOI: 10.1021/acs.bioconjchem.6b00102
Bioconjugate Chem. 2016, 27, 1153−1164

Previous studies in the literature have resulted in conflicting conclusions on the tumor targeting mechanism of nanoparticles, and the factors that govern the targeting property of nanoparticles are poorly understood. Nanconstruct **NP3-^{67}Ga** displays a remarkably higher cellular internalization compared with that of **NP4-^{67}Ga**. However, this did not translate to the biological profile, as it was observed that both nanoconjugates have a similar tumor uptake. We decided to investigate the mechanism of these targeted nanoparticles and performed blocking experiments, wherein the receptors were blocked by free peptide prior to the administration of the BBN-conjugated AuNPs. No difference in tumor uptake was observed. These results suggest that an active targeting mechanism is not playing a key role. Therefore, we believe that other factors, such as EPR and protein corona, influence the transport mechanism of targeted AuNPs to reach tumor. Aiming to obtain further understanding on whether the BBN-conjugated AuNPs recognize receptors *in vivo*, we performed experiments in which the nanoparticles were injected close to organs, other than the tumor, that express receptors for the bombesin peptide. It is very well known that the pancreas in mice overexpresses GRP receptors, and therefore, we administered **NP3-^{67}Ga** through the i.p. route. The i.p. injection provided AuNPs in close proximity to the receptors present in the pancreas.

Our results suggest that the **NP3-^{67}Ga** interaction seems to occur with the GRP receptors in the pancreas. These nanoconstructs showed up to 3% ID/g more in the pancreas compared with nontargeted ones (**NP2-^{67}Ga**). To further probe this hypothesis, we blocked the receptors with free bombesin. Here, we observed a decrease of ∼2.5 to 3% in **NP3-^{67}Ga** uptake in tumors. Taken together, it appears that active targeting plays a role: BBN nanoconjugates target GRP receptors in the pancreas, and BBN nanoconjugates showed more uptake in tumors than nontargeted nanoparticles. However, receptor blocking experiments reveal that uptake of the BBN-conjugated AuNPs in tumors is mediated by a passive mechanism. The contribution of both mechanisms operate in targeting of the AuNPs to tumors. However, the results pointed out that the BBN-conjugated AuNPs are not utilizing the receptor-mediated pathway as the primary route for targeting tumors, with the EPR pathway most probably playing a predominant role. In the case of i.p. administration, the nanoconjugates travel a longer distance to reach tumors than to reach intraperitoneal or retroperitoneal organs. Hence, they have a better chance of getting involved in interactions with circulating serum proteins during their way to the tumor sites, which may cause the corona effect. In brief, it is our reasoning that the receptor-mediated pathway *in vivo* is outweighed by the passive EPR effect or even hindered due to the possible formation of a protein corona enveloping the nanoparticles. In summary, both active and passive targeting play a role in governing the final *in vivo* fate of peptide conjugated nanoparticles. However, it is our reasoning that the significance of these mechanisms is highly dependent on the nanoparticle structure and its physicochemical properties. Our results encourage further evaluation of these nanoconstructs, considering their proven suitability to retain a stable coordination of $^{67}Ga^{3+}$ in a biological milieu. We anticipate that such suitability will also apply to other medically relevant trivalent radiometals, such as ^{111}In, ^{90}Y, or ^{177}Lu just to cite a few, conferring a high potential to this newly synthesized AuNPs in the design of multimodal tools for cancer theranostics. To fully explore this possibility, still it is crucial to provide the nanoparticle structure with the means to overcome its inability to optimally reach the desired target tumor with adequate payload.

EXPERIMENTAL PROCEDURES

All details of materials and methods including experimental procedures are provided in the Supporting Information.

ASSOCIATED CONTENT

Supporting Information

The Supporting Information is available free of charge on the ACS Publications website at DOI: 10.1021/acs.bioconjchem.6b00102.

Experimental procedures (PDF)

AUTHOR INFORMATION

Corresponding Authors

*(M.P.C.C.) E-mail: pcampelo@ctn.tecnico.ulisboa.pt.
*(A.P.) E-mail: apaulo@ctn.tecnico.ulisboa.pt.
*(R.K.) Department of Radiology, One Hospital Dr., Columbia, MO 65211, USA. E-mail: kannanr@health.missouri.edu.

Author Contributions

○F.S. and A.Z. contributed equally to this work.

Notes

The authors declare no competing financial interest.

ACKNOWLEDGMENTS

R.K. kindly acknowledges the "Michael J. and Sharon R. Bukstein Chair in Cancer Research" for financial support. R.K. thanks Coulter Foundation for providing financial support. Fundação para a Ciência e Tecnologia (FCT) is acknowledged for financial support (EXCL/QEQ-MED/0233/2012). C^{2}TN/IST authors gratefully acknowledge the FCT support through the UID/Multi/04349/2013 project and COST Action TD1004. C. Fernandes is acknowledged for the ESI-MS analyses which were run on a QITMS instrument acquired with the support of the Programa Nacional de Reequipamento Científico (Contract REDE/1503/REM/2005 - ITN) of FCT and is part of RNEM - Rede Nacional de Espectrometria de Massa. A.M.F. thanks Professor A. M. Botelho do Rego for the discussion of XPS results and also FCT for financial support of PEst-OE/CTM/LA0024/2013. F.S. thanks FCT for the doctoral research grant (SFRH/BD/47308/2008).

REFERENCES

(1) Chanda, N., Kattumuri, V., Shukla, R., Zambre, A., Katti, K., Upendran, A., Kulkarni, R. R., Kan, P., Fent, G. M., Casteel, S. W., et al. (2010) Bombesin functionalized gold nanoparticles show in vitro and in vivo cancer receptor specificity. *Proc. Natl. Acad. Sci. U. S. A. 107*, 8760−5.

(2) Chanda, N., Shukla, R., Katti, K. V., and Kannan, R. (2009) Gastrin releasing protein receptor specific gold nanorods: breast and prostate tumor avid nanovectors for molecular imaging. *Nano Lett. 9*, 1798−805.

(3) Brannon-Peppas, L., and Blanchette, J. O. (2004) Nanoparticle and targeted systems for cancer therapy. *Adv. Drug Delivery Rev. 56*, 1649−59.

(4) Dreaden, E. C., Mackey, M. A., Huang, X. H., Kang, B., and El-Sayed, M. A. (2011) Beating cancer in multiple ways using nanogold. *Chem. Soc. Rev. 40*, 3391−3404.

DOI: 10.1021/acs.bioconjchem.6b00102
Bioconjugate Chem. 2016, 27, 1153−1164

(5) Peer, D., Karp, J. M., Hong, S., FarokHzad, O. C., Margalit, R., and Langer, R. (2007) Nanocarriers as an emerging platform for cancer therapy. *Nat. Nanotechnol. 2*, 751−760.
(6) Master, A. M., and Sen Gupta, A. (2012) EGF receptor-targeted nanocarriers for enhanced cancer treatment. *Nanomedicine (London, U. K.) 7*, 1895−906.
(7) Kudgus, R. A., Walden, C. A., McGovern, R. M., Reid, J. M., Robertson, J. D., and Mukherjee, P. (2014) Tuning pharmacokinetics and biodistribution of a targeted drug delivery system through incorporation of a passive targeting component. *Sci. Rep. 4*, 5669.
(8) Bhattacharyya, S., Bhattacharya, R., Curley, S., McNiven, M. A., and Mukherjee, P. (2010) Nanoconjugation modulates the trafficking and mechanism of antibody induced receptor endocytosis. *Proc. Natl. Acad. Sci. U. S. A. 107*, 14541−6.
(9) Huang, X., Peng, X., Wang, Y., Wang, Y., Shin, D. M., El-Sayed, M. A., and Nie, S. (2010) A reexamination of active and passive tumor targeting by using rod-shaped gold nanocrystals and covalently conjugated peptide ligands. *ACS Nano 4*, 5887−96.
(10) Dreaden, E. C., Austin, L. A., Mackey, M. A., and El-Sayed, M. A. (2012) Size matters: gold nanoparticles in targeted cancer drug delivery. *Ther. Delivery 3*, 457−78.
(11) Hirn, S., Semmler-Behnke, M., Schleh, C., Wenk, A., Lipka, J., Schaffler, M., Takenaka, S., Möller, W., Schmid, G., Simon, U., et al. (2011) Particle size-dependent and surface charge-dependent biodistribution of gold nanoparticles after intravenous administration. *Eur. J. Pharm. Biopharm. 77*, 407−16.
(12) Verma, A., and Stellacci, F. (2010) Effect of Surface Properties on Nanoparticle-Cell Interactions. *Small 6*, 12−21.
(13) Arvizo, R. R., Miranda, O. R., Moyano, D. F., Walden, C. A., Giri, K., Bhattacharya, R., Robertson, J. D., Rotello, V. M., Reid, J. M., and Mukherjee, P. (2011) Modulating pharmacokinetics, tumor uptake and biodistribution by engineered nanoparticles. *PLoS One 6*, e24374.
(14) Arvizo, R. R., Miranda, O. R., Thompson, M. A., Pabelick, C. M., Bhattacharya, R., Robertson, J. D., Rotello, V. M., Prakash, Y. S., and Mukherjee, P. (2010) Effect of nanoparticle surface charge at the plasma membrane and beyond. *Nano Lett. 10*, 2543−8.
(15) Khan, J. A., Kudgus, R. A., Szabolcs, A., Dutta, S., Wang, E., Cao, S., Curran, G. L., Shah, V., Curley, S., Mukhopadhyay, D., et al. (2011) Designing nanoconjugates to effectively target pancreatic cancer cells in vitro and in vivo. *PLoS One 6*, e20347.
(16) Aggarwal, P., Hall, J. B., McLeland, C. B., Dobrovolskaia, M. A., and McNeil, S. E. (2009) Nanoparticle interaction with plasma proteins as it relates to particle biodistribution, biocompatibility and therapeutic efficacy. *Adv. Drug Delivery Rev. 61*, 428−37.
(17) Wolfram, J., Yang, Y., Shen, J., Moten, A., Chen, C., Shen, H., Ferrari, M., and Zhao, Y. (2014) The nano-plasma interface: Implications of the protein corona. *Colloids Surf., B 124*, 17−24.
(18) Wang, Y., Liu, Y., Luehmann, H., Xia, X., Brown, P., Jarreau, C., Welch, M., and Xia, Y. (2012) Evaluating the pharmacokinetics and in vivo cancer targeting capability of Au nanocages by positron emission tomography imaging. *ACS Nano 6*, 5880−8.
(19) Perrault, S. D., Walkey, C., Jennings, T., Fischer, H. C., and Chan, W. C. (2009) Mediating tumor targeting efficiency of nanoparticles through design. *Nano Lett. 9*, 1909−15.
(20) Perrault, S. D., and Chan, W. C. (2010) In vivo assembly of nanoparticle components to improve targeted cancer imaging. *Proc. Natl. Acad. Sci. U. S. A. 107*, 11194−9.
(21) Kodiha, M., Wang, Y. M., Hutter, E., Maysinger, D., and Stochaj, U. (2015) Off to the organelles - killing cancer cells with targeted gold nanoparticles. *Theranostics 5*, 357−70.
(22) Zhou, J., and Rossi, J. J. (2014) Cell-type-specific, Aptamer-functionalized Agents for Targeted Disease Therapy. *Mol. Ther.–Nucleic Acids 3*, e169.
(23) Ding, Y., Jiang, Z., Saha, K., Kim, C. S., Kim, S. T., Landis, R. F., and Rotello, V. M. (2014) Gold nanoparticles for nucleic acid delivery. *Mol. Ther. 22*, 1075−83.
(24) Rana, S., Bajaj, A., Mout, R., and Rotello, V. M. (2012) Monolayer coated gold nanoparticles for delivery applications. *Adv. Drug Delivery Rev. 64*, 200−16.
(25) Bhattacharyya, S., Singh, R. D., Pagano, R., Robertson, J. D., Bhattacharya, R., and Mukherjee, P. (2012) Switching the targeting pathways of a therapeutic antibody by nanodesign. *Angew. Chem., Int. Ed. 51*, 1563−7.
(26) Kirpotin, D. B., Drummond, D. C., Shao, Y., Shalaby, M. R., Hong, K., Nielsen, U. B., Marks, J. D., Benz, C. C., and Park, J. W. (2006) Antibody targeting of long-circulating lipidic nanoparticles does not increase tumor localization but does increase internalization in animal models. *Cancer Res. 66*, 6732−40.
(27) Bartlett, D. W., Su, H., Hildebrandt, I. J., Weber, W. A., and Davis, M. E. (2007) Impact of tumor-specific targeting on the biodistribution and efficacy of siRNA nanoparticles measured by multimodality in vivo imaging. *Proc. Natl. Acad. Sci. U. S. A. 104*, 15549−54.
(28) Maina, T., Nock, B., and Mather, S. (2006) Targeting prostate cancer with radiolabelled bombesins. *Cancer Imaging 6*, 153−7.
(29) Abd-Elgaliel, W. R., Gallazzi, F., Garrison, J. C., Rold, T. L., Sieckman, G. L., Figueroa, S. D., Hoffman, T. J., and Lever, S. Z. (2008) Design, synthesis, and biological evaluation of an antagonist-bombesin analogue as targeting vector. *Bioconjugate Chem. 19*, 2040−8.
(30) Biddlecombe, G. B., Rogers, B. E., de Visser, M., Parry, J. J., de Jong, M., Erion, J. L., and Lewis, J. S. (2007) Molecular imaging of gastrin-releasing peptide receptor-positive tumors in mice using 64Cu- and 86Y-DOTA-(Pro1,Tyr4)-bombesin(1−14). *Bioconjugate Chem. 18*, 724−30.
(31) Lin, K. S., Luu, A., Baidoo, K. E., Hashemzadeh-Gargari, H., Chen, M. K., Brenneman, K., Pili, R., Pomper, M., Carducci, M. A., and Wagner, H. N., Jr. (2005) A new high affinity technetium-99m-bombesin analogue with low abdominal accumulation. *Bioconjugate Chem. 16*, 43−50.
(32) Banerjee, S. R., and Pomper, M. G. (2013) Clinical applications of Gallium-68. *Appl. Radiat. Isot. 76*, 2−13.
(33) Suresh, D., Zambre, A., Chanda, N., Hoffman, T. J., Smith, C. J., Robertson, J. D., and Kannan, R. (2014) Bombesin peptide conjugated gold nanocages internalize via clathrin mediated endocytosis. *Bioconjugate Chem. 25*, 1565−79.
(34) Shirmardi, S. P., Gandomkar, M., Maragheh, M. G., and Shamsaei, M. (2011) Preclinical evaluation of a new bombesin analog for imaging of gastrin-releasing peptide receptors. *Cancer Biother.Radiopharm. 26*, 309−16.
(35) Chen, Q., Ma, Q., Chen, M., Chen, B., Wen, Q., Jia, B., Wang, F., Sun, B., and Gao, S. (2015) An exploratory study on 99mTc-RGD-BBN peptide scintimammography in the assessment of breast malignant lesions compared to 99mTc-3P4-RGD2. *PLoS One 10*, e0123401.
(36) Faintuch, B. L., Teodoro, R., Duatti, A., Muramoto, E., Faintuch, S., and Smith, C. J. (2008) Radiolabeled bombesin analogs for prostate cancer diagnosis: preclinical studies. *Nucl. Med. Biol. 35*, 401−11.
(37) Sano, K., Okada, M., Hisada, H., Shimokawa, K., Saji, H., Maeda, M., and Mukai, T. (2013) In vivo evaluation of a radiogallium-labeled bifunctional radiopharmaceutical, Ga-DOTA-MN2, for hypoxic tumor imaging. *Biol. Pharm. Bull. 36*, 602−8.
(38) Hnatowich, D. J., Friedman, B., Clancy, B., and Novak, M. (1981) Labeling of preformed liposomes with Ga-67 and Tc-99m by chelation. *J. Nucl. Med. 22*, 810−4.
(39) Wadas, T. J., Wong, E. H., Weisman, G. R., and Anderson, C. J. (2010) Coordinating radiometals of copper, gallium, indium, yttrium, and zirconium for PET and SPECT imaging of disease. *Chem. Rev. 110*, 2858−902.
(40) Shanehsazzadeh, S., Oghabian, M. A., Lahooti, A., Abdollahi, M., Haeri, S. A., Amanlou, M., Daha, F. J., and Allen, B. J. (2013) Estimated background doses of [Ga-67]-DTPA-USPIO in normal Balb/c mice as a potential therapeutic agent for liver and spleen cancers. *Nucl. Med. Commun. 34*, 915−925.

DOI: 10.1021/acs.bioconjchem.6b00102
Bioconjugate Chem. 2016, 27, 1153−1164

(41) Alric, C., Taleb, J., Le Duc, G., Mandon, C., Billotey, C., Le Meur-Herland, A., Brochard, T., Vocanson, F., Janier, M., Perriat, P., et al. (2008) Gadolinium chelate coated gold nanoparticles as contrast agents for both X-ray computed tomography and magnetic resonance imaging. *J. Am. Chem. Soc. 130*, 5908−5915.
(42) Shan, L. (2010) Gold Nanoparticles Coated with Dithiolated Diethylenetriamine Pentaacetic Acid-Gadolinium Chelate, in *Molecular Imaging and Contrast Agent Database (MICAD)*, National Center for Biotechnology Information, Bethesda, MD.
(43) Zambre, A., Silva, F., Upendran, A., Afrasiabi, Z., Xin, Y., Paulo, A., and Kannan, R. (2014) Synthesis and characterization of functional multicomponent nanosized gallium chelated gold crystals. *Chem. Commun. (Cambridge, U. K.) 50*, 3281−4.
(44) Debouttiere, P. J., Roux, S., Vocanson, F., Billotey, C., Beuf, O., Favre-Reguillon, A., Lin, Y., Pellet-Rostaing, S., Lamartine, R., Perriat, P., et al. (2006) Design of gold nanoparticles for magnetic resonance imaging. *Adv. Funct. Mater. 16*, 2330−2339.
(45) Brust, M., Walker, M., Bethell, D., Schiffrin, D. J., and Whyman, R. (1994) Synthesis of thiol-derivatized gold nanoparticles in a 2-phase liquid-liquid system. *J. Chem. Soc., Chem. Commun. 0*, 801−802.
(46) Albanese, A., Tang, P. S., and Chan, W. C. W. (2012) The Effect of Nanoparticle Size, Shape, and Surface Chemistry on Biological Systems. *Annu. Rev. Biomed. Eng. 14*, 1−16.
(47) Lindner, S., Michler, C., Wangler, B., Bartenstein, P., Fischer, G., Schirrmacher, R., and Wangler, C. (2014) PESIN Multimerization Improves Receptor Avidities and in Vivo Tumor Targeting Properties to GRPR-Overexpressing Tumors. *Bioconjugate Chem. 25*, 489−500.
(48) Nam, H. Y., Kwon, S. M., Chung, H., Lee, S. Y., Kwon, S. H., Jeon, H., Kim, Y., Park, J. H., Kim, J., Her, S., et al. (2009) Cellular uptake mechanism and intracellular fate of hydrophobically modified glycol chitosan nanoparticles. *J. Controlled Release 135*, 259−267.
(49) Rejman, J., Oberle, V., Zuhorn, I. S., and Hoekstra, D. (2004) Size-dependent internalization of particles via the pathways of clathrin- and caveolae-mediated endocytosis. *Biochem. J. 377*, 159−69.
(50) Oh, N., and Park, J. H. (2014) Endocytosis and exocytosis of nanoparticles in mammalian cells. *Int. J. Nanomed. 9* (Suppl 1), 51−63.
(51) Kannan, R., Rahing, V., Cutler, C., Pandrapragada, R., Katti, K. K., Kattumuri, V., Robertson, J. D., Casteel, S. J., Jurisson, S., Smith, C., et al. (2006) Nanocompatible chemistry toward fabrication of target-specific gold nanoparticles. *J. Am. Chem. Soc. 128*, 11342−3.
(52) Pombo Garcia, K., Zarschler, K., Barbaro, L., Barreto, J. A., O'Malley, W., Spiccia, L., Stephan, H., and Graham, B. (2014) Zwitterionic-coated "stealth" nanoparticles for biomedical applications: recent advances in countering biomolecular corona formation and uptake by the mononuclear phagocyte system. *Small 10*, 2516−29.
(53) Zhao, Y., Sultan, D., Detering, L., Cho, S., Sun, G., Pierce, R., Wooley, K. L., and Liu, Y. (2014) Copper-64-alloyed gold nanoparticles for cancer imaging: improved radiolabel stability and diagnostic accuracy. *Angew. Chem., Int. Ed. 53*, 156−9.
(54) Varasteh, Z., Velikyan, I., Lindeberg, G., Sorensen, J., Larhed, M., Sandstrom, M., Selvaraju, R. K., Malmberg, J., Tolmachev, V., and Orlova, A. (2013) Synthesis and characterization of a high-affinity NOTA-conjugated bombesin antagonist for GRPR-targeted tumor imaging. *Bioconjugate Chem. 24*, 1144−53.
(55) Schuhmacher, J., Zhang, H., Doll, J., Macke, H. R., Matys, R., Hauser, H., Henze, M., Haberkorn, U., and Eisenhut, M. (2005) GRP receptor-targeted PET of a rat pancreas carcinoma xenograft in nude mice with a 68Ga-labeled bombesin(6−14) analog. *J. Nucl. Med. 46*, 691−9.
(56) Dijkgraaf, I., Franssen, G. M., McBride, W. J., D'Souza, C. A., Laverman, P., Smith, C. J., Goldenberg, D. M., Oyen, W. J., and Boerman, O. C. (2012) PET of tumors expressing gastrin-releasing peptide receptor with an 18F-labeled bombesin analog. *J. Nucl. Med. 53*, 947−52.
(57) Kannan, R., Pillarsetty, N., Gali, H., Hoffman, T. J., Barnes, C. L., Jurisson, S. S., Smith, C. J., and Volkert, W. A. (2011) Design and synthesis of a bombesin peptide-conjugated tripodal phosphino dithioether ligand topology for the stabilization of the fac-[M(CO)3]+ core (M = (99 m)Tc or Re). *Inorg. Chem. 50*, 6210−9.
(58) Sasidharan, A., Riviere, J. E., and Monteiro-Riviere, N. A. (2015) Gold and silver nanoparticle interactions with human proteins: impact and implications in biocorona formation. *J. Mater. Chem. B 3*, 2075−2082.
(59) Berret, J. F. (2007) Stoichiometry of electrostatic complexes determined by light scattering. *Macromolecules 40*, 4260−4266.
(60) Peng, Q., Zhang, S., Yang, Q., Zhang, T., Wei, X. Q., Jiang, L., Zhang, C. L., Chen, Q. M., Zhang, Z. R., and Lin, Y. F. (2013) Preformed albumin corona, a protective coating for nanoparticles based drug delivery system. *Biomaterials 34*, 8521−30.
(61) Salvati, A., Pitek, A. S., Monopoli, M. P., Prapainop, K., Bombelli, F. B., Hristov, D. R., Kelly, P. M., Aberg, C., Mahon, E., and Dawson, K. A. (2013) Transferrin-functionalized nanoparticles lose their targeting capabilities when a biomolecule corona adsorbs on the surface. *Nat. Nanotechnol. 8*, 137−143.
(62) Gaspar, R. (2013) Nanoparticles: Pushed off target with proteins. *Nat. Nanotechnol. 8*, 79−80.
(63) Chen, F., Hong, H., Shi, S., Goel, S., Valdovinos, H. F., Hernandez, R., Theuer, C. P., Barnhart, T. E., and Cai, W. (2014) Engineering of hollow mesoporous silica nanoparticles for remarkably enhanced tumor active targeting efficacy. *Sci. Rep. 4*, 5080.

DOI: 10.1021/acs.bioconjchem.6b00102
Bioconjugate Chem. 2016, 27, 1153−1164